

Jessica Zhou, Yue Cao, James Balter, Neeraj Chaudhary,
Aditya S. Pandey, Greg Thompson, and Christina I. Tsien

Introduction

Stereotactic radiosurgery (SRS) involves the delivery of a very precise, focal dose of radiation to a target. Radiologic imaging is crucial for accurate delineation of the treatment volume in order to achieve maximal dose to the target and optimal sparing of the normal surrounding tissue. Conventional imaging reflects only anatomic rather than functional properties of the tumor. In contrast, metabolic and physiologic imaging provides in vivo measures of tumor tissue properties. In this chapter, physiologic MR imaging techniques including proton spectroscopy, blood volume, blood flow, vascular permeability, diffusion, and diffusion tensor imaging, as well as metabolic PET imaging, will be described. Although SRS treatment has been established for many years, recent advances in modern imaging combined with improved radiotherapy techniques can provide better target definition, reduce normal tissue toxicity, and provide better assessment of treatment response. This chapter describes the role of novel MR and PET imaging in the treatment planning and posttreatment follow-up of both malignant and benign central nervous system (CNS) intracranial tumors.

J. Zhou, M.D. • Y. Cao, M.D. • J. Balter, Ph.D.
Department of Radiation Oncology, University of Michigan
Hospital and Health Systems, Ann Arbor, MI, USA

N. Chaudhary, M.D., M.R.C.S., F.R.C.R.
Departments of Radiology & Neurosurgery, University of
Michigan, Neuro-interventional Radiology, Ann Arbor, MI, USA

A.S. Pandey, M.D. • G. Thompson, M.D.
Department of Neurosurgery, University of Michigan
Hospital and Health Systems, Ann Arbor, MI, USA

C.I. Tsien, M.D. (✉)
Department of Radiation Oncology, Washington University in
St. Louis, 4921 Parkview Place, Campus Box 8224,
St. Louis, MO 63110, USA
e-mail: ctsien@radonc.wustl.edu

Imaging and Treatment Planning Considerations

Conventional contrast-enhanced computed tomography (CT) scanning provides anatomic as well as electron density information with sufficient geometric accuracy to support stereotactic targeting and to calculate dose. MR contrast-enhanced T1-weighted and T2-weighted imaging provides superior soft tissue contrast relative to imaging and has also been routinely used in target volume definition for SRS of intracranial tumors.

In order to combine the advantages of MRI and CT, it has been historically necessary to spatially register these images within the treatment planning system (Fig. 2.1). Image registration permits accurate mapping of imaging data from other modalities to a single coordinate system, typically the treatment planning CT scan [1].

MRI Alone for SRS Simulation and Planning

More recently, MRI has been used as a stand-alone modality for SRS treatment planning. Traditionally 1.5 T MR scanners have been used for this purpose. There is increasing interest now in the use of 3 T MR scanners, which have a higher signal to noise ratio and consequently higher spatial resolution and shorter image acquisition time. A recent study by Zhang et al. showed that the geometric accuracy achieved with 3 T MRI is comparable to 1.5 T MRI for SRS treatment planning [2]. The advantage of MRI-based planning is that it removes systematic errors that may occur due to CT-MRI registration and eliminates radiation exposure from the CT scan. However, this must be balanced against potential disadvantages of omitting the CT scan including possible spatial distortion of the MRI scan due to gradient field nonlinearity and magnetic field inhomogeneities, the lack of electron density information used for dose calculation, and the difficulty in patient setup verification during treatment delivery [3]. MRI simulation

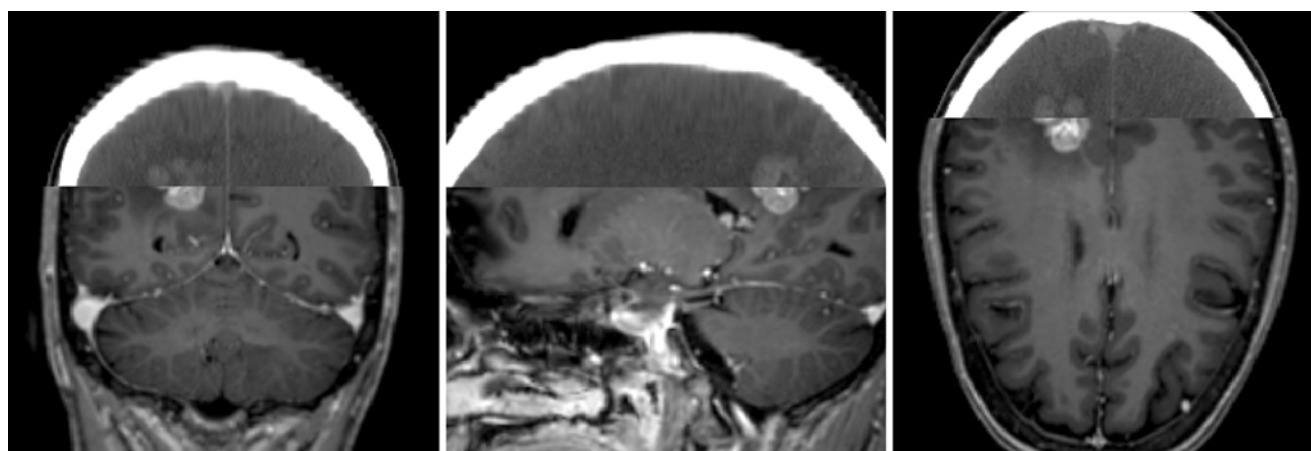


Fig. 2.1 Split window display of image registration of MR and CT for a right parietal brain metastasis for SRS treatment planning in the axial (*right image*), sagittal (*middle image*), and coronal (*left image*) views

may also require a larger bore for patient setup to allow for appropriate MRI compatible immobilization devices.

Solutions to these shortcomings of MRI-based plans are being developed. The lack of an identifiable relationship between MR image values and electron densities has been addressed in a variety of ways. Early treatment planning using MRI alone involved assignment of bulk densities (e.g., to bone and the rest of the brain), which resulted in a smaller (1–1.5 %) calculated dose difference between the MRI-based and a CT-based plans when compared to plans without bulk density assignment. More recent work has included use of electron density atlases and statistical modeling of tissue composition to assign attenuation properties. Recent developments which may benefit MRI–PET systems as well as radiation oncology include ultrashort TE (UTE) imaging and even more sophisticated attenuation models [4, 5]. These methods may reduce uncertainties of MR planning in most regions of the brain to a fairly insignificant level in the near future. One issue of note, however, is the potential for local distortion effects, e.g., due to air–tissue interfaces, which may cause displacements of 1–2 mm over very short distances from the interface (<1 cm) [6].

Radiologic and Anatomic Considerations During Treatment Planning

The goal of SRS is not only to give a maximal dose of focal radiation to the target but also to prevent injury to the surrounding normal tissue. Both tumor size and proximity to surrounding structures need to be taken into consideration during treatment planning.

Tumor size dictates the feasibility of radiosurgery. Increasing tumor size results in an exponential increase in the margin of normal brain tissue irradiated and is potentially associated with a higher risk of complications. Results from

the RTOG 9005 trial showed significantly higher CNS toxicity in patients with larger tumor diameters [7]. Tumors with diameters between 2.1 and 3 cm have a 7.3-fold increased risk of developing toxicity over tumors with diameters of 2 cm or less. Tumors between 3.1 and 4 cm had a 16-fold increased risk. In general, SRS is recommended for tumors less than 4 cm in size [7].

The safety of SRS and the rates of post-treatment complication can also vary based on the location of the tumor relative to the surrounding cerebral structures. In a review by Flickinger et al., the rate of symptomatic radiation necrosis was highest (threefold increased risk) for arteriovenous malformation (AVM) lesions in the basal ganglia and the brainstem (pons, midbrain, medulla) [8]. In contrast, the risk of radiation injury remained low (even with increased volumes) for lesions irradiated in the frontal and temporal lobes.

Similarly, the proximity of critical neuroanatomic structures to the targeted area is important to consider during SRS planning. Relative contraindications for SRS include close proximity or involvement of the optic tract including the optic nerves and chiasm. The optic apparatus dose is generally limited to 10 Gy to limit the risk of optic neuropathy [9, 10]. In contrast, the remaining cranial nerves have somewhat higher dose tolerances [11, 12].

Physiologic MR Imaging and Metabolic PET Imaging in SRS

Physiologic MR and metabolic PET imaging can add to information obtained by morphological imaging and serve as a surrogate marker for specific biologic processes. These imaging techniques permit in vivo analysis of tumor tissue properties including chemical composition, tumor vasculature, perfusion, and tumor cellularity [13].

Assessing tumor response after SRS can be difficult due to occurrence of early nonspecific imaging changes that can represent either recurrent or progressive tumor, or treatment-related inflammatory and/or necrotic changes such as areas of contrast enhancement and edema on T1-weighted imaging. Underlying processes of radiation injury cause a temporary increase in contrast enhancement on MRI, termed “pseudoprogression,” making the differentiation between true progression and radiation effects extremely difficult. Mechanisms that may contribute to radiation-induced neurotoxicity include vascular injury, glial and white matter changes, and immunological mechanisms.

Advanced MR imaging techniques are now becoming routinely available and will continue to play an increasingly important role in aiding in the precise definition of at risk target volumes as well as the assessment of treatment response [14–16]. In this section, a brief overview of these imaging techniques will be described.

Dynamic Susceptibility Contrast MRI

Dynamic susceptibility contrast (DSC) T2*-weighted imaging is the preferred method to map whole-brain perfusion properties [17–19]. Dynamic acquisition of T2*-weighted MR imaging during intravenous injection of Gd-DTPA allows estimations of cerebral (tumor) blood volume (CBV), cerebral (tumor) blood flow (CBF), and mean bolus transit time (MTT). These parameters can be measured in the imaged volume by mathematical deconvolution of the arterial input function (from a cerebral artery) and the tissue response signal. These perfusion parameters provide assessment of tumor viability, tumor vascular properties, and transport kinetics following therapy [13]. Several studies have shown a correlation between cerebral blood volume and the histological grade of the tumor [20, 21].

Dynamic Contrast-Enhanced MRI

Dynamic contrast-enhanced (DCE), MR imaging using T1-weighted imaging provides a method for quantitative assessment of tumor vascular permeability. DCE MRI is obtained following dynamic acquisition over several minutes during intravenous injection of a bolus of Gd-GTPA. Estimations of vascular permeability with DCE MRI require the application of pharmacokinetic models with an arterial input function and therefore are more complex than CBV estimation. DCE MRI has been shown to be important in assessment of treatment response following both anti-angiogenic agents and radiation [22].

MR Spectroscopy Imaging

MR spectroscopy is a technique to detect proton metabolites in tissue, *in vivo*. This imaging technique provides information regarding tumor proliferation, cell membrane breakdown, neuronal activity, and tumor necrosis [15, 23]. Most commonly detected metabolites include choline-containing compounds, creatine, lactate, lipid, and N-acetylaspartate. Spectroscopic images are obtained with either two-dimensional or three-dimensional means of acquisition. This is achieved by mapping the concentration of each of the compounds within voxel sizes of approximately 1 cm³. Malignant tumors are characterized by an elevated choline to N-acetyl aspartate (NAA) ratio due to greater cell membrane phospholipid turnover from increased tumor proliferation as well as decreased NAA compared to the normal brain [24, 25]. Several studies have demonstrated the utility of MR spectroscopy in pretreatment evaluation and radiotherapy planning as well as in differentiating radiation necrosis from recurrent tumor [26–28].

MR Diffusion and Diffusion Tensor Imaging

Diffusion MRI measures the mobility of water within tissues at the cellular level and therefore can detect microenvironment changes in tumor tissue. Changes in diffusion can occur due to cell swelling, necrotic/apoptotic cell death after therapy, or extracellular water space changes as a result of edema [29]. Changes in tumor such as cytolytic cell death following successful therapy lead to transient increases in regional diffusion, which may be an important early indicator of treatment response. The extent of directional diffusion can be estimated with an apparent diffusion coefficient (ADC). Diffusion has traditionally been analyzed using average ADC values throughout an entire tumor, which can significantly underestimate regional changes following therapy [30]. The parametric response map (PRM_{ADC}) has been developed as a voxel-wise approach for evaluating ADC changes and has been found to be an independent, early predictor of overall survival [31]. ADC maps are largely independent of the MRI system, vendor, and field strength. Therefore, it provides an accurate and noninvasive method of performing longitudinal studies [32].

Diffusion tensor imaging (DTI) is a diffusion technique that allows visualization of white matter architecture and has been increasingly investigated as an imaging biomarker for detecting physiological changes prior to any changes on conventional imaging [33]. Previous studies have suggested that changes in diffusion index of normal appearing brain white

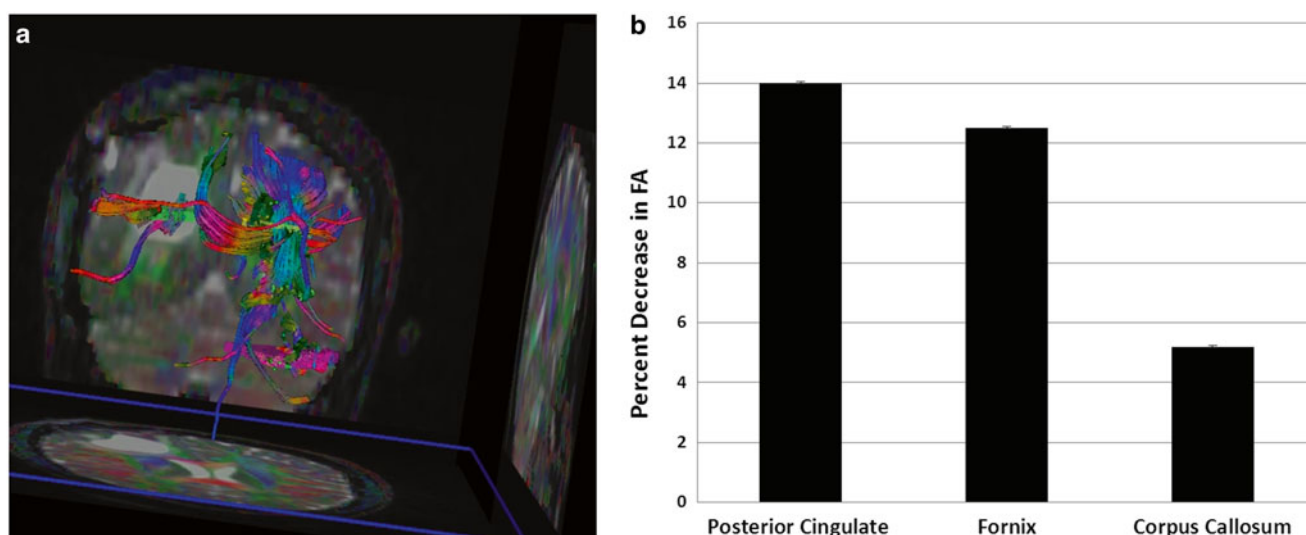


Fig. 2.2 (a) MR diffusion tensor imaging and tractography illustrating a right parietal–occipital mass and the bilateral corticospinal tracts. Peritumoral edema appears to infiltrate and displace the posterior and superior part of the right corticospinal tract compared to the left. (b) Quantitative DTI analyses were performed on specific white matter structures including the posterior cingulate, fornix, and corpus callosum. Fractional anisotropy (FA) values in the

cingulum and fornix show significant decreases compared to the corpus callosum 1 month following radiation, suggesting increased radiation sensitivity. Preliminary data showing a correlation between early diffusivity changes and late decline in verbal recall suggest that DTI imaging may be a useful biomarker for late CNS toxicity [34]. Means and standard errors of the percentage decrease in FA 1 month post-RT are plotted

matter structures following radiation may also be an indicator for delayed radiation-induced neurotoxicity [34]. These studies examined changes in diffusion indices including fractional anisotropy (FA) as an index of fiber integrity, mean diffusivity (MD) as an index of overall diffusivity, radial diffusivity (RD) as an index of demyelination, and axial diffusivity (AD) as an index of fiber degradation [35]. Surgical series have demonstrated the utility of DTI in reducing the risk of morbidity of brain tumor resections near critical structures. Similar incorporation of DTI tractography imaging in SRS may be valuable with regards to delineation of normal tissue avoidance structures in treatment planning for lesions near eloquent regions (Fig. 2.2) [36]. Incorporation of tractography data in SRS treatment planning has been shown in studies to lead to decreased dose to critical structures including the optic tract and pyramidal tracts [37].

Metabolic PET Imaging

With a number of tracer compounds available, PET and SPECT allow for noninvasive measurements of tumor hypoxia, proliferation index, and markers of apoptosis [38, 39]. The cellular and physiological information obtained may be used in combination with MR imaging, which still has relatively superior spatial resolution, to improve target volume definition in radiotherapy planning [40].

¹¹C Methionine (MET)-PET visualizes increased radio-tracer uptake by metabolically active tumor. It is able to detect increased cellular metabolism in brain tumors involving

increased protein transport mediated by L-type amino acid carriers at the blood–brain barrier level compared with normal brain tissue [41]. It is able to better differentiate tumor from background brain signals than ¹⁸F-labeled 2-fluoro-2-deoxy-D-glucose (FDG)-PET, which is more difficult to interpret due to the high level of intrinsic glucose uptake in the brain.

¹⁸F-fluorothymidine (FLT)-PET uses the alternative tracer FLT, which is a thymidine analogue that is incorporated exclusively into DNA. This allows measurement of the activity of cellular thymidine kinase, which increases several folds as cells enter the S phase and begin DNA synthesis. Therefore, increased FLT uptake is a direct measure of cellular proliferation rate and correlates with Ki-67 staining [42].

Imaging Consideration in the SRS Treatment of Malignant Tumors

Brain Metastases

Whole-brain radiotherapy has been the mainstay of treatment of brain metastasis. However, there has been a recent shift toward greater use of stereotactic radiosurgery in patients with a limited number of brain metastases and with controlled systemic disease in order to increase dose to tumor and minimize neurocognitive morbidity [43].

SRS target volume definition for brain metastasis is typically accomplished using conventional thin-cut CT or T1-weighted MR imaging with contrast enhancement.

Studies have reported on improved outcomes with the addition of a 1–2 mm margin to account for microscopic disease in the SRS treatment of brain metastases [44, 45]. The additional margin may be necessary to account for possible infiltrative tumor growth beyond the enhancing border as well as the limited accuracy of delineation of the enhancing border based on current imaging methods. A study by Baumert et al. evaluated specimens from 76 metastatic brain lesions and found that 63 % of the specimens showed tumor infiltration beyond the metastases boundary, with small-cell lung cancer and melanoma showing a maximum depth of infiltration of >1 mm and other histologies <1 mm [45]. Non-small cell lung cancer, melanoma, and sarcoma also showed the most number of infiltration zones outside the boundary. Another study by Noel et al. found that the addition of a 1 mm margin on MRI to account for microscopic disease extension for brain metastases improved the 2-year local control rate from 51 to 90 % [44].

SRS is also frequently used as adjuvant treatment to maximize local control following surgical resection, with reported control rates of approximately 80 % [46]. In planning treatment in the adjuvant setting, one also needs to take into consideration changes in the size of the surgical cavity when delineating the target volume. In a study by Atalar et al. on 68 lesions, the postresection cavity volume was smaller than the preresection tumor volume by a median percent volume change of 29 % [47]. The authors found that the greatest volume change occurred immediately after surgery during postoperative days 0–3, with no significant change occurring up to 33 days after surgery. Thus, there may not be a benefit to an extended waiting period prior to proceeding with SRS. A planning margin for microscopic extension has also been shown to improve control in the adjuvant setting. A study by Soltys et al. analyzed 76 resection cavities that were treated with radiosurgery [48]. Less conformal treatment plans with a 2.4 mm margin of brain tissue around the cavity had a 100 % local control rate, compared with 78 % for a 1.7 mm margin, 52 % for 1.5 mm, and 43 % for 0.8 mm. Toxicity was minimal and therefore the inclusion of a 2 mm margin to improve local control was recommended.

Assessment of Treatment Response

Novel imaging techniques in addition to conventional contrast-enhanced MRI are now more frequently used to assess brain metastasis response following radiosurgery.

MR diffusion imaging has been used in the evaluation of SRS treatment response (Fig. 2.3). Several studies have noted that longitudinal ADC values may be important in predicting early tumor response to SRS treatment. In a prospective study by Huang et al., 21 patients with 32 brain metastases were analyzed. ADCs were measured both prior

and following SRS [49]. ADC values for the group showing radiation-induced central necrosis was significantly higher than those demonstrating recurrent tumor growth. Similar results were noted in a prospective trial of 38 patients treated with gamma knife radiosurgery for brain metastases with significant increases in mean ADC values indicative of stable disease and unchanged ADC levels indicative of tumor recurrence [50]. The changes in ADC occurred before any definitive change in volume were evident on further imaging studies. In another study, posttreatment ADC patterns compared with initial diffusion imaging were used to predict ultimate treatment outcomes on serial MR imaging in 25 metastatic tumors [51]. The authors found that the normalized ADC patterns outperformed initial posttreatment tumor volume in predicting long-term response to treatment.

At the University of Michigan, alterations in vascular volume and permeability in brain metastases, as measured using dynamic contrast-enhanced MRI have been analyzed to predict subsequent volumetric response following radiation. In a recent prospective study that evaluated 43 lesions from 20 patients, results showed that the percentage decrease in the high-CBV-defined subvolumes of the tumor was greater in the group of responsive tumors than in the group of stable and progressive tumors ($P < 0.007$). Perfusion changes were a significantly better predictor for post-RT response than changes in the gross tumor volume observed during the same time interval ($P = 0.012$), suggesting that physiological changes occur prior to volumetric changes [52].

PET imaging, including FDG PET, has also been evaluated for differentiating between recurrence and posttreatment changes. Studies have shown that areas of radiation injury have lower glucose metabolism than normal brain tissue due to lower cellular attenuation [53]. Varying degrees of accuracy of FDG-PET in detecting tumor recurrence versus radiation necrosis have been reported. Several retrospective analyses have shown sensitivity in detection of tumor recurrence ranging from 80 to 100 % and specificity higher than 80 %; however, these studies lacked histopathological validation [54, 55]. In a study of 15 patients with a histopathologically confirmed diagnosis, Thompson et al. showed that FDG-PET was sufficiently sensitive to differentiate recurrent tumor from radiation effect in only 43 % of the cases and was least accurate when the lesion volume was less than 6 cm³ [56].

MET-PET may provide a better method for differentiating radiation necrosis from recurrent tumor. In 21 patients with suspected recurrent metastatic brain tumor or radiation injury, MET-PET scans showed a sensitivity of 78 % and specificity of 100 % in detecting tumor recurrence [57]. In another study of 77 patients, a mean SUV ratio of lesion uptake to contralateral normal gray matter uptake of greater than 1.41 provided the best sensitivity (79 %) and specificity (75 %) for metastatic brain tumor and a value of greater than 1.58 provided the best sensitivity (75 %) and specificity (75 %) for recurrent glioma [58].

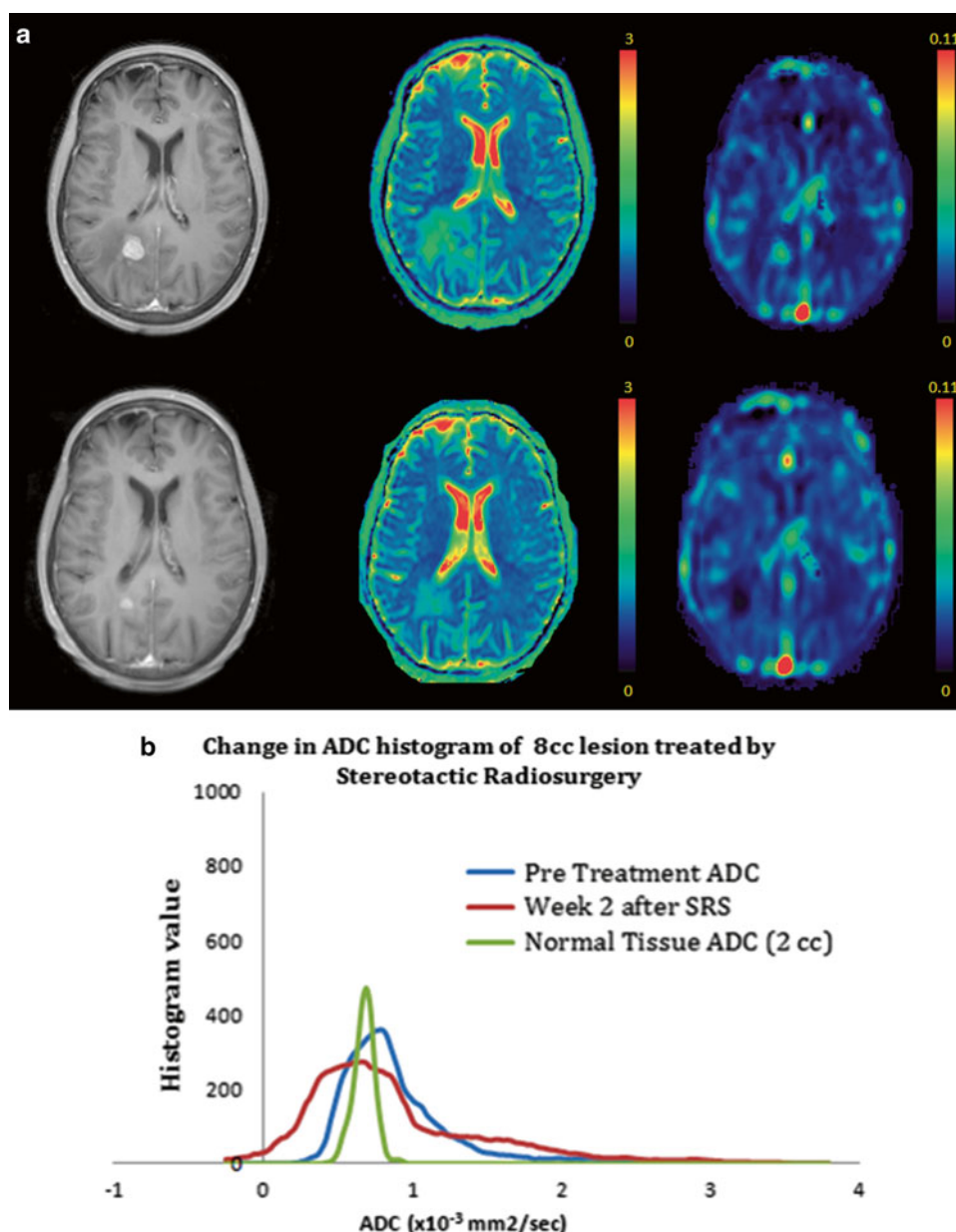


Fig. 2.3 (a) T1-weighted images (*right*), ADC map (*middle*), and perfusion map (*left*) are shown at baseline prior to SRS for a right parietal brain metastases (*top row*) and 1 month post SRS treatment (*bottom row*). Qualitatively, there are significant decreases noted in tumor volume, diffusion, and perfusion 1 month after treatment. (b) Mean ADC histogram analyses performed for the normal tissue

(*green*), a region of interest corresponding to a brain metastases at baseline (*blue*) and 2 weeks after SRS (*red*). Quantitative ADC histogram analysis demonstrate the fractional tumor subvolume with low ADC appeared to increase 2 weeks after SRS consistent with a nonresponsive or progressive tumor confirmed on subsequent follow-up imaging at 4 months

Recurrent Gliomas

SRS has been increasingly used as a potential treatment option for recurrent gliomas in combination with anti-angiogenic agents following an initial course of standard fractionation of RT in combination [59].

Novel imaging techniques can be utilized in treatment planning, especially in cases where there is no tissue confirmation of recurrent disease (Fig. 2.4). MR spectroscopy has been

shown to potentially improve target delineation. Areas of contrast enhancement on T1-weighted conventional MRI do not always correspond to the most aggressive areas as reflected by high choline concentration. The extent of elevated choline has been found beyond the tumor volume defined by Gd enhancement or hyperintense lesions on T2-weighted or FLAIR images [60, 61]. Several studies have suggested that elevated choline peaks correlate with higher tumor grade. In a study of 247 tissue specimens from 31 untreated patients with low- or

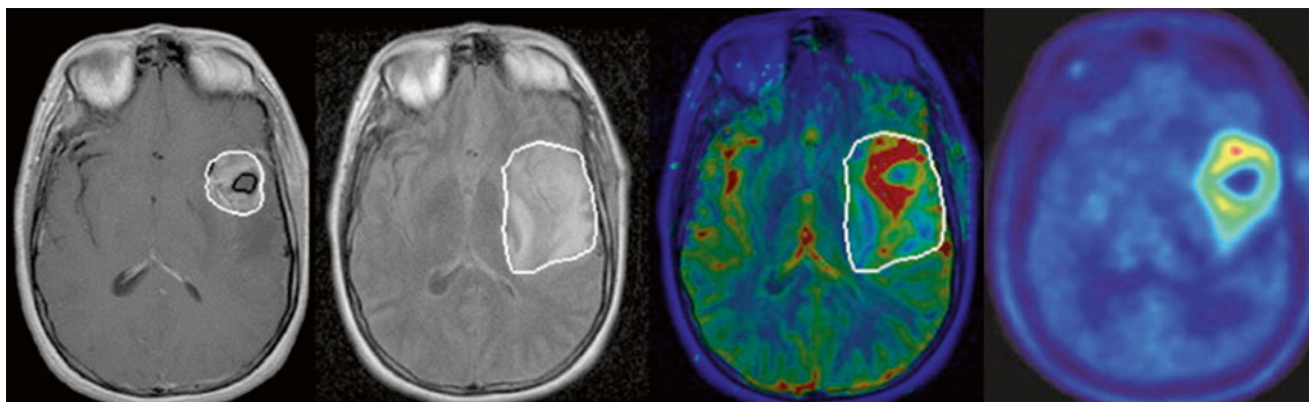


Fig. 2.4 Multimodality MR imaging for target volume definition for a left temporal glioblastoma. T1 post-gadolinium notes a contrast-enhancing lesion (*far left image*) with significant peritumoral edema shown on MR FLAIR imaging (*second image from left*). Perfusion map shows areas of high CBV (*red*) extending beyond the contrast-enhancing tumor rim as

defined by T1 post-gad (*third image from left*). This shows the potential for perfusion MRI to identify aggressive subvolumes in gliomas [11]. C MET PET (*far right image*) also provides additional information for target volume definition compared with conventional MR regarding tumor extension along the white matter tract

high-grade glioma, choline peak height normalized to contralateral creatine and choline or ipsilateral NAA significantly correlated with tumor cell density [62].

The degree of spatial overlap between tumor volumes with elevated choline and the radiosurgical target volume has been correlated with clinical outcome. A retrospective study in patients with recurrent GBMs treated with SRS found an improvement in survival if the target volume overlapped with the pretreatment MR spectroscopy metabolic lesion by 50 % or greater (median OS 15.7 versus 10.4 months, $P < 0.01$) [63].

Newer imaging techniques are also crucial in posttreatment follow-up of recurrent gliomas as posttreatment contrast-enhancing lesions often consist of a mixture of tumor cells and tissue with radiation injury and therefore are difficult to accurately differentiate noninvasively.

MR spectroscopy is one modality that is being increasingly used to distinguish the two in the posttreatment setting. However, there is currently no consensus in the literature on which calculated ratios can best differentiate tumor recurrence from radiation injury. One study of 100 tissue biopsy samples from 44 patients with grade 2–4 gliomas, a choline/NAA ratio cutoff threshold of 2.5, was able to differentiate recurrent tumor from normal, edematous, and necrotic brain tissue, with an approximate 90 % sensitivity and 86 % specificity [64]. Another study showed the ability to differentiate tumor recurrence from radiation injury in 27 of 28 patients by using a cutoff value of 1.8 or greater for the choline/NAA or choline/creatine ratio representing tumor recurrence [28].

MR perfusion imaging has also shown its utility in post SRS treatment evaluation. One study prospectively evaluated 42 image-guided tissue specimens from 13 patients with high-grade glioma using threshold relative CBV values to distinguish recurrent tumor from radiation changes [65]. The authors found that the treatment-related group

had relative CBV values from 0.21 to 0.71, while the recurrent tumor group had CBV values from 0.55 to 4.64. A threshold value of 0.71 therefore optimized differentiation between the two groups with a sensitivity of 91.7 % and specificity of 100 %.

Imaging Considerations in the SRS Treatment of Benign Lesions

Acoustic Neuroma (Vestibular Schwannomas)

Acoustic neuromas are benign neoplasms derived from Schwann cells of the myelin sheath that show a predilection for involvement of sensory nerves. Acoustic neuromas account for approximately 5–8 % of intracranial tumors and 80–90 % of cerebellopontine angle tumors. Retrospective data have shown excellent tumor control rates with stereotactic radiosurgery [66]. A University of Pittsburgh study of 216 patients with unilateral acoustic neuromas treated with Gamma knife (marginal tumor dose of 12–13 Gy) showed a 10 year resection-free control rate of 98.3 %, low toxicity with good rates of hearing preservation (Robertson–Gardner serviceable hearing 45 %), and high preservation rates of trigeminal and facial nerve function [67].

Contrast-enhanced MRI is used to evaluate treatment response. Following SRS treatment, clinical data suggest that acoustic neuromas may temporarily expand in size initially and then stabilize. Thus, a longer period of follow-up is required before determining disease progression. A retrospective review of 75 patients showed that 23 % had evidence of pseudoprogression with onset of enlargement at 6 months, of which 9 % remained larger than initial volume at last follow-up. No further progression was seen beyond 24 months for all patients [68]. Another study involving 87 patients showed that peak

tumor volume expansion was observed at 8.6 months after SRS [69]. At 5 years follow-up, the mean reduction in tumor volume was 31 %. However, there were still 10 % of tumors that remained larger than their initial volume.

Considering the potential for pseudoprogression, follow-up recommendations include posttreatment MR imaging to establish a baseline and at 24 months, followed by yearly imaging. In general, salvage therapy is not recommended before 2 years unless there is clinical deterioration.

Hydrocephalus can also be seen on follow-up imaging, a potential complication following SRS treatment of acoustic neuromas. In a retrospective review of 444 patients treated with radiosurgery, symptomatic communicating hydrocephalus developed in 5.6 % of patients, with a median time to symptom development of 7 months [70]. Patient monitoring for development of hydrocephalus is recommended following SRS treatment for up to 3–4 years.

Trigeminal Neuralgia

Trigeminal neuralgia is a painful syndrome resulting in intense and often severe episodes of lancinating pain occurring in the distribution of cranial nerve V. Although benign, trigeminal neuralgia can significantly diminish a patients' quality of life. Common treatment options include antiepileptics, neuroleptics, opioids, and antidepressant medications. When medication fails to alleviate the effects of trigeminal neuralgia, available treatments include microvascular surgical decompression, ablation, and SRS. SRS has been highly successful in pain control, with excellent response in 70–90 % of patients [71]. In a prospective clinical trial, 100 patients were treated with Gamma Knife radiosurgery to a median dose of 85 Gy [72]. Of the total, 83% of the patients were pain free at a minimum follow-up time of 12 months and 70 % had stopped taking medications during the study. Post treatment complications were minimal, with facial paresthesia in 6 % and hypesthesia in 4 %.

MRI is of paramount importance for the accurate planning of SRS treatment of trigeminal neuralgia. Studies have shown relatively limited use of imaging in predicting effective treatment outcome because the evidence of treatment benefit or treatment failure is most often readily apparent before enhancement occurs. Posttreatment follow-up with contrast-enhanced MRI taken at 6 months can provide for target confirmation due to the high prevalence of contrast enhancement. The posttreatment imaging characteristics of trigeminal neuralgia were assessed by Massager et al., who reported that at 6 months post-treatment, contrast enhancement on T1-weighted MRI was seen in 83 % of trigeminal nerve roots [73]. However, they found no correlation between the occurrence of focal enhancement of the nerve root and pain outcome, or development of trigeminal dysfunction. Repeated serial imaging is generally not considered helpful

in those patients who did not initially present with radiologic or neurologic changes on the initial posttreatment scan. Nor is serial repeat imaging recommended for those patients who respond well clinically unless neurological deficits emerge. Imaging may be used for the assessment of potential radiation-related injury to the brainstem.

Arteriovenous Malformations

Arteriovenous malformations (AVMs) are abnormal communications between arteries and veins, usually associated with high blood flow that results in blood vessel remodeling. The incidence of AVMs is approximately 0.01–0.1 %, and presenting symptoms include hemorrhage, seizure, and headaches. The average annual risk of bleeding is 2–3 %, with a slightly higher risk if there is a prior history of bleed (2–6 %) and slightly lower risk if no prior bleed (1–3 %) [74]. AVMs are graded based on the Spetzler–Martin scale, which reflects the size and venous drainage, as well as eloquence of the adjacent brain. Current treatment options include surgery, with operability depending on AVM location, embolization, and SRS.

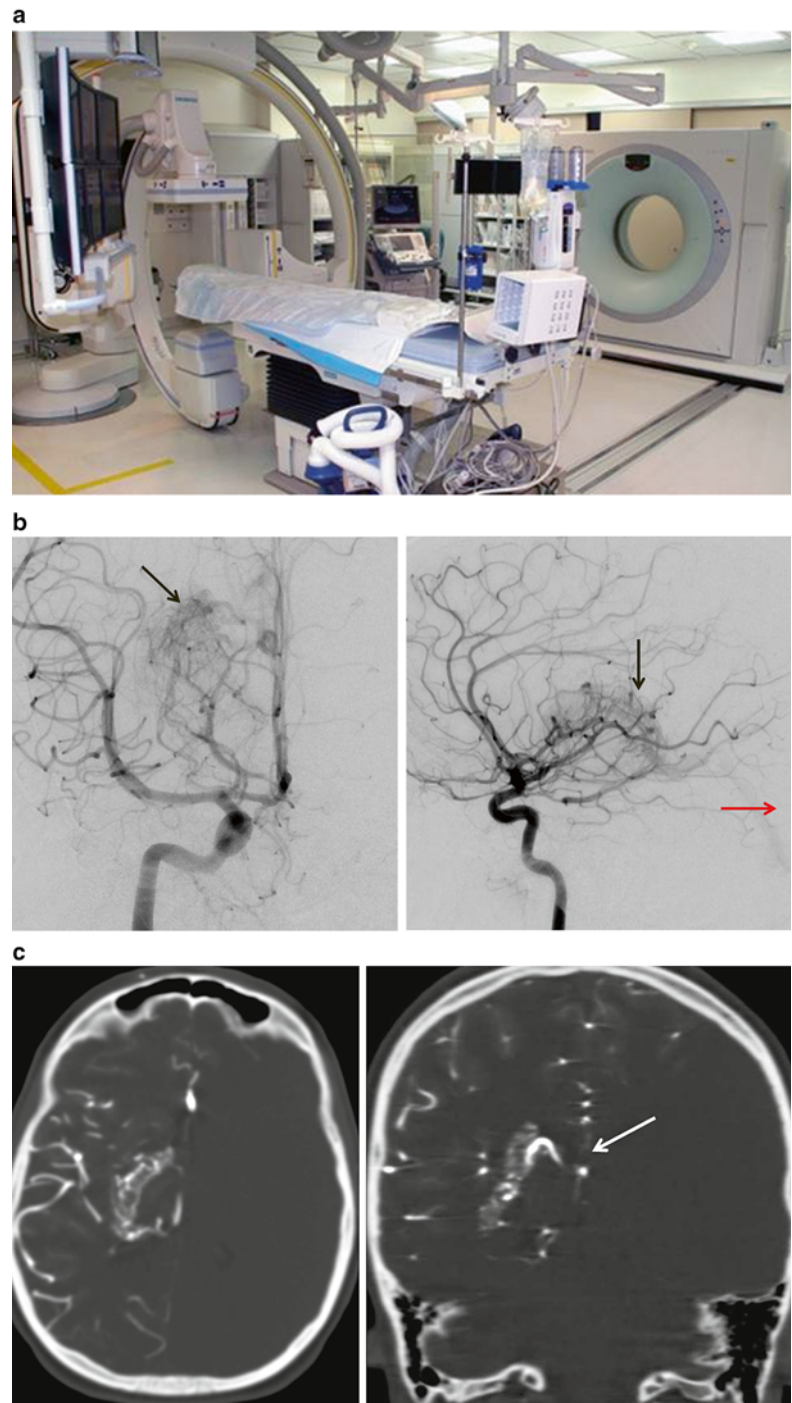
Following SRS, clinical studies show obliteration rates of 60–90 % [75, 76]. In one study, 351 patients were treated to a median dose of 20 Gy, and the rate of obliteration was 73 % by angiography, 86 % by MR alone, and 75 % overall [77]. A persistent out-of-field nidus was seen in 18 % of previously embolized and 5 % of nonembolized pts. Data on larger AVMs show decreasing obliteration and higher complication rates with increasing volume.

Although SRS is noninvasive, one disadvantage of SRS compared with surgery is the potential for continued risk of hemorrhage in the 1–3 years after treatment. A retrospective observational study of 500 patients on the rates of hemorrhage showed that, compared with the period between diagnosis and radiosurgery, the risk of hemorrhage decreased by 54 % during a median latency period of 2 years from treatment to angiographic evidence of obliteration and by 88 % after angiographic obliteration [78].

Cerebral Angiography

Cerebral angiography has been the gold standard in the initial diagnosis and evaluation of AVMs, as part of radiosurgery treatment planning, and in posttreatment residual AVM monitoring [79, 80]. It is a dynamic, real-time study that shows not only the presence or absence of an AVM but also the vascular transit time. It provides superior spatial resolution without overlap of adjacent vascular structures as would be seen on CT or MRI. The image acquisition on cerebral angiography is rapid and enables delineation of the arterial and venous phases of the circulation, which allows better visualization of the AVM nidus and its shunt components. The potential complications of the invasive procedure include stroke, arterial dissection, and reactions to the contrast agent.

Fig. 2.5 (a) University of Michigan Hybrid CT and biplane digital subtraction angiography (DSA) suite; (b) Intra-arterial CT angiography showing the nidus of a right-sided basal ganglia AVM in both the axial (*left image*) and coronal plane (*right image*). (c) Deep venous drainage is noted by the white arrow in the coronal plane (*right image*)



Even though angiography is useful as a diagnostic tool in defining the nidus, feeding arteries and draining veins, it is limited in its use for radiosurgery treatment planning purposes because of its 2D dataset. This can lead to both over- and underestimation of the AVM nidus in the target volume [81]. Alternate approaches include obtaining either intravenous CTA or MRI angiography to provide a 3D view of the nidus [82]. Most recently, hybrid biplane angiography and CT-on-rails suites have been developed for the safe

placement of endovascular catheters and subsequent capture of cross-sectional vascular imaging with an intra-arterial CTA technique [83]. Together, the high spatial and temporal resolution of biplane angiography can be combined with the relatively high-contrast soft tissue resolution of CT imaging. Small cerebral AVMs are often not readily seen on IV-CTA or MRA and instead may require high-resolution intra-arterial CTA images that may provide better target volume delineation for SRS treatment planning (Fig. 2.5).

AVM Radiosurgery Treatment Planning

The primary goal of AVM radiosurgery is to develop a plan with a target volume that conforms closely to the surface of the AVM nidus while maintaining a steep dose gradient to minimize the radiation dose to the surrounding brain. More recently, tractography has been used in the AVM setting to identify better accuracy areas at risk in the brain that can cause patient morbidity if compromised [84]. A prospective study by Koga et al. integrated tractography in 71 AVM radiosurgery treatments where the tumor was less than 1 cm from fiber tracts including the pyramidal tract, optic tract, and the arcuate fasciculus. Morbidity as a result of treatment was minimized, with only one patient experiencing permanent and one experiencing transient pyramidal tract dysfunction [85].

Post AVM Follow-Up Imaging

MR perfusion imaging has been used to assess response following SRS. In a study by Guo et al., perfusion relative cerebral blood volume (rCBV) and cerebral blood flow (rCBF) maps were assessed in 19 patients before and after radiosurgery [86]. Prior to treatment, the ratio of rCBV and rCBF of the ipsilateral hemisphere to the unaffected hemisphere was found to be significantly higher in patients with AVM than those of healthy patients, consistent with a cerebral steal phenomenon. After treatment, starting at 6 months follow-up, the ratio of rCBV and rCBF of the AVM nidus to normal brain gradually decreased to 1.0. Decrease was also seen in the hemispheric perfusion ratios, reflecting reversal of steal toward normal perfusion.

Currently, the standard for posttreatment follow-up of AVMs is MRI every year with cerebral angiography for confirmation of obliteration of the nidus. An angiographic cure requires that no nidus or shunting is identified on the follow-up imaging study.

Conclusion

Novel functional and metabolic MRI and PET imaging provides the ability to analyze tumor tissue properties including chemical composition, vasculature and perfusion, water mobility, permeability, hypoxia, and tumor proliferation. These imaging modalities have the potential to improve radiosurgery treatment planning and posttreatment monitoring, including evaluation of differences in treatment efficacy between patients and heterogeneity of response within tumors. Further investigation in randomized studies is warranted to better integrate these imaging techniques into routine clinical practice.

References

1. Petti PL, Kessler ML, Fleming T, Pitluck S, et al. An automated image-registration technique based on multiple structure matching. *Med Phys.* 1994;21(9):1419–26.
2. Zhang B, MacFadden D, Damyanovich AZ, Rieker M, Stainsby J, Bernstein M, Jaffray DA, Mikulis D, Menard C. Development of a geometrically accurate imaging protocol at 3T MRI for SRS treatment planning. *Phys Med Biol.* 2010;55(22):6601–15.
3. Pinnaduwa D. MRI-based simulation and treatment planning: are we there yet? [Internet]. 2012 [updated 2012 Mar 17, cited 2013 Jan 22]. Available from: <http://www.ucsfcmf.com/2012/slides/MRO12001/16PinnaduwaMRSimulationAndPlanningAreWeThereYet.pdf>.
4. Johansson A, Karlsson M, Nyholm T. CT substitute derived from MRI sequences with ultrashort echo time. *Med Phys.* 2011;38(5):2708–14.
5. Keereman V, Fierens Y, Broux T, De Deene Y, Lonnewux M, Vandenbergh S. MRI-based attenuation correction for PET/MRI using ultrashort echo time sequences. *J Nucl Med.* 2010;51(5):812–8.
6. Wang H, Balter J, Cao Y. Patient-induced susceptibility effect on geometric distortion of clinical brain MRI for radiation treatment planning on a 3T scanner. *Phys Med Biol.* 2013;58(3):465–77.
7. Shaw E, Scott C, Souhami L, Dinapoli R, Kline R, Loeffler J, Farnan N. Single dose radiosurgical treatment of recurrent previously irradiated primary brain tumors and brain metastases: final report of RTOG protocol 90–05. *Int J Radiat Oncol Biol Phys.* 2000;47(2):291–8.
8. Flickinger JC, Kondiolka D, Lunsford LD, Kassam A, Phuong LK, Liscak R, Pollock B. Development of a model to predict permanent symptomatic postradiosurgery injury for arteriovenous malformation patients. *Int J Radiat Oncol Biol Phys.* 2000;46(5):1143–8.
9. Tishler RB, Loeffler JS, Lunsford LD, Duma C, Alexander 3rd E, Kooy HM, Flickinger JC. Tolerance of cranial nerves of the cavernous sinus to radiosurgery. *Int J Radiat Oncol Biol Phys.* 1993;27(2):215–21.
10. Leber KA, Bergloff J, Pendl G. Dose-response tolerance of the visual pathways and cranial nerves of the cavernous sinus to stereotactic radiosurgery. *J Neurosurg.* 1998;88(1):43–50.
11. Morita A, Coffey RJ, Foote RL, Schiff D, Gorman D. Risk of injury to cranial nerves after gamma knife radiosurgery for skull base meningiomas: experience in 88 patients. *J Neurosurg.* 1999;90(1):42–9.
12. Foote KD, Friedman WA, Buatti JM, Meeks SL, Bova FJ, Kubilis PS. Analysis of risk factors associated with radiosurgery for vestibular schwannoma. *J Neurosurg.* 2001;95(3):440–9.
13. Cao Y, Sundgren PC, Tsien CI, Chenevert TT, Junck L. Physiologic and metabolic magnetic resonance imaging in gliomas. *J Clin Oncol.* 2006;24(8):1228–35.
14. Zakian KL, Koutcher JA, Ballon D, Hricak H, Ling CC. Developments in nuclear magnetic resonance imaging and spectroscopy: application to radiation oncology. *Semin Radiat Oncol.* 2001;11(1):3–15.
15. Nelson SJ. Multivoxel magnetic resonance spectroscopy of brain tumors. *Mol Cancer Ther.* 2003;2(5):497–507.
16. Pardo FS, Aronen HJ, Kennedy D, Moulton G, Paiva K, Okunieff P, Schmidt EV, Hochberg FH, Harsh GR, Fischman AJ. Functional cerebral imaging in the evaluation and radiotherapeutic treatment planning of patients with malignant glioma. *Int J Radiat Oncol Biol Phys.* 1994;30(3):663–9.
17. Paulson ES, Schmainda KM. Comparison of dynamic susceptibility-weighted contrast-enhanced MR methods: recommendations for measuring relative cerebral blood volume in brain tumors. *Radiology.* 2008;249(2):601–13.

18. Maeda M, Itoh S, Kimura H, Iwasaki T, Hayashi N, Yamamoto K, Ishii Y, Kubota T. Tumor vascularity in the brain: evaluation with dynamic susceptibility-contrast MR imaging. *Radiology*. 1993;189(1):233–8.
19. Thomsen H, Steffensen E, Larsson EM. Perfusion MRI (dynamic susceptibility contrast imaging) with different measurement approaches for the evaluation of blood flow and blood volume in human gliomas. *Acta Radiol*. 2012;53(1):95–101.
20. Roberts HC, Roberts TP, Brasch RC, Dillon WP. Quantitative measurement of microvascular permeability in human brain tumors achieved using dynamic contrast-enhanced MR imaging: correlation with Histologic grade. *AJNR Am J Neuroradiol*. 2000;21(5):891–9.
21. Provenzale JM, Wang GR, Brenner T, Petrella JR, Sorensen AG. Comparison of permeability in high-grade and low-grade brain tumors using dynamic susceptibility contrast MR imaging. *AJR Am J Roentgenol*. 2002;178(3):711–6.
22. Morgan B, Thomas AL, Dreys J, Hennig J, Buchert M, Jivan A, Horsfield MA, Mross K, Ball HA, Lee L, Mietlowski W, Fuxius S, Unger C, O'Byrne K, Henry A, Cherryman GR, Laurent D, Dugan M, Marme D, Steward WP. Dynamic contrast-enhanced magnetic resonance imaging as a biomarker for the pharmacological response of PTK787/ZK 222584, an inhibitor of the vascular endothelial growth factor receptor tyrosine kinases, in patients with advanced colorectal cancer and liver metastases: results from two phase I studies. *J Clin Oncol*. 2003;21(21):3955–64.
23. Preul MC, Caramanos Z, Collins DL, Villemure JG, Leblanc R, Olivier A, Pokrupa R, Arnold DL. Accurate, noninvasive diagnosis of human brain tumors by using proton magnetic resonance spectroscopy. *Nat Med*. 1996;2(3):323–5.
24. Wald LL, Nelson SJ, Day MR, Noworolski SE, Henry RG, Huhn SL, Chang S, Prados MD, Sneed PK, Larson DA, Wara WM, McDermott M, Dillon WP, Gutin PH, Vigneron DB. Serial proton magnetic resonance spectroscopy imaging of glioblastoma multiforme after brachytherapy. *J Neurosurg*. 1997;87(4):525–34.
25. Negendank WG, Sauter R, Brown TR, Evelhoch JL, Falini A, Gotsis ED, Heerschap A, Kamada K, Lee BC, Mengeot MM, Moser E, Padavic-Schaller KA, Sanders JA, Spraggins TA, Stillman AE, Terwey B, Vogl TJ, Wicklow K, Zimmerman RA. Proton magnetic resonance spectroscopy in patients with glial tumors: a multicenter study. *J Neurosurg*. 1996;84(3):449–58.
26. Einstein DB, Wessels B, Bangert B, Fu P, Nelson AD, Cohen M, Sagar S, Lewin J, Sloan A, Zheng Y, Williams J, Colussi V, Vinkler R, Maciunas R. Phase II trial of radiosurgery to magnetic resonance spectroscopy-defined high-risk tumor volumes in patients with glioblastoma multiforme. *Int J Radiat Oncol Biol Phys*. 2012;84(3):668–74.
27. Huang J, Wang AM, Shetty A, Maitz AH, Yan D, Doyle D, Richey K, Park S, Pieper DR, Chen PY, Grills IS. Differentiation between intra-axial metastatic tumor progression and radiation injury following fractionated radiation therapy or stereotactic radiosurgery using MR spectroscopy, perfusion MR imaging or volume progression modeling. *Magn Reson Imaging*. 2011;29(7):993–1001.
28. Weybright P, Sundgren PC, Maly PV, Hassan DG, Nan B, Rohrer S, Junck L. Differentiation between brain tumor recurrence and radiation injury using MR spectroscopy. *AJR Am J Roentgenol*. 2005;185(6):1471–6.
29. Hamstra DA, Galban CJ, Meyer CR, Johnson TD, Sundgren PC, Tsien C, Lawrence TS, Junck L, Ross DJ, Rehemtulla A, Ross BD, Chenevert TL. Functional diffusion map as an early imaging biomarker for high-grade glioma: correlation with conventional radiologic response and overall survival. *J Clin Oncol*. 2008;26(20):3387–94.
30. Galban CJ, Chenevert TL, Meyer CR, Tsien C, Lawrence TS, Hamstra DA, Junck L, Sundgren PC, Johnson TD, Ross DJ, Rehemtulla A, Ross BD. The parametric response map is an imaging biomarker for early cancer treatment outcome. *Nat Med*. 2009;15(5):572–6.
31. Moffat BA, Chenevert TL, Lawrence TS, Meyer CR, Johnson TD, Dong Q, Tsien C, Mukherji S, Quint DJ, Gebarski SS, Robertson PL, Junck LR, Rehemtulla A, Ross BD. Physiologic diffusion map: a noninvasive MRI biomarker for early stratification of clinical brain tumor response. *Proc Natl Acad Sci U S A*. 2005;102(15):5524–9.
32. Malyarenko D, Galban CJ, Londy FJ, Meyer C, Johnson TD, Rehemtulla A, Ross BD, Chenevert TL. Multi-system repeatability and reproducibility of apparent diffusion coefficient measurement using an ice-water phantom. *J Magn Reson Imaging*. 2013;37(5):1238–46.
33. Nagesh V, Tsien CI, Chenevert TL, Ross BD, Lawrence TS, Junck L, Cao Y. Radiation-induced changes in normal-appearing white matter in patients with cerebral tumors: a diffusion tensor imaging study. *Int J Radiat Oncol Biol Phys*. 2008;70(4):1002–2010.
34. Chapman CH, Nagesh V, Sundgren PC, Buchtel H, Chenevert TL, Junck L, Lawrence TS, Tsien CI, Cao Y. Diffusion tensor imaging of normal-appearing white matter as biomarker for radiation-induced late delayed cognitive decline. *Int J Radiat Oncol Biol Phys*. 2012;82(5):2033–40.
35. Nazem-Zadeh MR, Jafari-Khouzani K, Davoodi-Bojd E, Jiang Q, Soltanian-Zadeh H. Clustering method for estimating principal diffusion directions. *Neuroimage*. 2011;57(3):825–38.
36. Yen PS, Teo BT, Chiu CH, Chen SC, Chiu TL, Su CF. White Matter tract involvement in brain tumors: a diffusion tensor imaging analysis. *Surg Neurol*. 2009;72(5):464–9.
37. Pantelis E, Papadakis N, Verigos K, Stathochristopoulou I, Antypas C, Lekas L, Tzouras A, Georgiou E, Salvaras N. Integration of functional MRI and white matter tractography in stereotactic radiosurgery clinical practice. *Int J Radiat Oncol Biol Phys*. 2010;78(1):257–67.
38. Chao ST, Suh JH, Raja S, Lee SY, Barnett G. The sensitivity and specificity of FDG PET in distinguishing recurrent brain tumor from radionecrosis in patients treated with stereotactic radiosurgery. *Int J Cancer*. 2001;96(3):191–7.
39. Barthel H, Cleij MC, Collingridge DR, Hutchinson OC, Osman S, He Q, Luthra SK, Brady F, Price PM, Aboagye EO. 3'-deoxy-3'-[18F]fluorothymidine as a new marker for monitoring tumor response to antiproliferative therapy in vivo with positron emission tomography. *Cancer Res*. 2003;63(13):3791–8.
40. Grosu AL, Feldmann H, Dick S, Dzewas B, Nieder C, Gumprecht H, Frank A, Schwaiger M, Molls M, Weber WA. Implications of IMT-SPECT for postoperative radiotherapy planning in patients with gliomas. *Int J Radiat Oncol Biol Phys*. 2002;54(3):842–54.
41. Torii K, Tsuyuguchi N, Kawabe J, Sunada I, Hara M, Shiomi S. Correlation of amino-acid uptake using methionine PET and histological classifications in various gliomas. *Ann Nucl Med*. 2005;19(8):677–83.
42. Sato N, Suzuki M, Kuwata N, Kuroda K, Wada T, Beppu T, Sera K, Sasaki T, Ogawa A. Evaluation of the malignancy of glioma using 11C-Methionine positron emission tomography and proliferating cell nuclear antigen staining. *Neurosurg Rev*. 1999;22(4):210–4.
43. Kocher M, Soffietti R, Abacioglu U, Villa S, Fauchon F, Baumert BG, Fariselli L, Tzuk-Shina T, Kortmann RD, Carrie C, Ben Hassel M, Kouri M, Valeinis E, van den Berge D, Collette S, Collette L, Mueller RP. Adjuvant whole-brain radiotherapy versus observation after radiosurgery or surgical resection of one to three cerebral metastases: results of the EORTC 22952–26001 study. *J Clin Oncol*. 2011;29(2):134–41.
44. Baumert BG, Rutten I, Dehing-Oberije C, Twijnstra A, Dirx MJ, Debougnoux-Huppertz RM, Lambin P, Kubat B. A pathology-based substrate for target definition in radiosurgery of brain metastases. *Int J Radiat Oncol Biol Phys*. 2006;66(1):187–94.
45. Noel G, Simon JM, Valery CA, Cornu P, Boissier G, Hasboun D, Ledu D, Tep B, Delattre JY, Marsault C, Baillet F, Mazeran JJ. Radiosurgery for brain metastasis: impact of CTV on local control. *Radiother Oncol*. 2003;68(1):15–21.

46. Robbins JR, Ryu S, Kalkanis S, Cogan C, Rock J, Movsas B, Kim JH, Rosenblum M. Radiosurgery to the surgical cavity as adjuvant therapy for resected brain metastasis. *Neurosurgery*. 2012;71(5):937–43.
47. Atalar B, Choi CY, Harsh 4th GR, Chang SD, Gibbs IC, Adler JR, Soltys SG. Cavity volume dynamics after resection of brain metastases and timing of postresection cavity stereotactic radiosurgery. *Neurosurgery*. 2013;72(2):180–5.
48. Soltys SG, Adler JR, Lipani JD, Jackson PS, Choi CY, Puataweepong P, White S, Gibbs IC, Chang SD. Stereotactic radiosurgery of the postoperative resection cavity for brain metastases. *Int J Radiat Oncol Biol Phys*. 2008;70(1):187–93.
49. Huang CF, Chou HH, Yang MS, Lee JK, Lin LY. Diffusion magnetic resonance imaging as an evaluation of the response of brain metastases treated by stereotactic radiosurgery. *Surg Neurol*. 2008;69(1):62–8.
50. Huang CF, Chiou SY, Wu MF, Tu HT, Liu WS, Chuang JC. Apparent diffusion coefficients for evaluation of the response of brain tumors treated by Gamma Knife surgery. *J Neurosurg*. 2010;113(Suppl):97–104.
51. Goldman M, Boxerman JL, Rogg JM, Noren G. Utility of apparent diffusion coefficient in predicting the outcome of Gamma Knife-treated brain metastases prior to changes in tumor volume: a preliminary study. *J Neurosurg*. 2006;105(Suppl):175–82.
52. Farjam R, Tsien CI, Feng FY, Gomez-Hassan D, Hayman JA, Lawrence TS, Cao Y. Physiological imaging-defined response-driven subvolumes of a tumor. *Int J Radiat Oncol Biol Phys*. 2013;85(5):1383–90.
53. Di Chiro G, Oldfield E, Wright DC, De Michele D, Katz DA, Patronas NJ, Doppman JL, Larson SM, Ito M, Kufta CV. Cerebral necrosis after radiotherapy and/or intraarterial chemotherapy for brain tumors: PET and neuropathologic studies. *AJR Am J Roentgenol*. 1988;150(1):189–97.
54. Kim EE, Chung S-K, Haynie TP, Kim CG, Cho BJ, Podoloff DA, Tilbury RS, Yang DJ, Yung WK, Moser Jr RP, et al. Differentiation of residual or recurrent tumors from post-treatment changes in F-18 FDG-PET. *Radiographics*. 1992;12(2):269–79.
55. Ogawa T, Kanno I, Shishido F, Inugami A, Higano S, Fujita H, Murakami M, Uemura K, Yasui N, Mineura K. Clinical value of PET with [18F]fluorodeoxyglucose and L-methyl-11C-methionine for diagnosis of recurrent brain tumor and radiation injury. *Acta Radiol*. 1991;32(3):197–202.
56. Thompson TP, Lunsford LD, Kondziolka D. Distinguishing recurrent tumor and radiation necrosis with positron emission tomography versus stereotactic biopsy. *Stereotact Funct Neurosurg*. 1999;73(1–4):9–14.
57. Tsuyuguchi N, Sunada I, Iwai Y, Yamanaka K, Tanaka K, Takami T, Otsuka Y, Sakamoto S, Ohata K, Goto T, Hara M. Methionine positron emission tomography of recurrent metastatic brain tumor and radiation necrosis after stereotactic radiosurgery: is a differential diagnosis possible? *J Neurosurg*. 2003;98(5):1056–64.
58. Terakawa Y, Tsuyuguchi N, Iwai Y, Yamanaka K, Higashiyama S, Takami T, Ohata K. Diagnostic accuracy of 11C-methionine PET for differentiation of recurrent brain tumors from radiation necrosis after radiotherapy. *J Nucl Med*. 2008;49(5):694–9.
59. Cuneo KC, Vredenburgh JJ, Sampson JH, Reardon DA, Desjardins A, Peters KB, Friedman HS, Willett CG, Kirkpatrick JP. Safety and efficacy of stereotactic radiosurgery and adjuvant bevacizumab in patients with recurrent malignant gliomas. *Int J Radiat Oncol Biol Phys*. 2012;82(5):2018–24.
60. Li X, Lu Y, Pirzkall A, McKnight T, Nelson SJ. Analysis of the spatial characteristics of metabolic abnormalities in newly diagnosed glioma patients. *J Magn Reson Imaging*. 2002;16(3):229–37.
61. Pirzkall A, Li X, Oh J, Chang S, Berger MS, Larson DA, Verhey LJ, Dillon WP, Nelson SJ. 3D MRSI for resected high-grade gliomas before RT: tumor extent according to metabolic activity in relation to MRI. *Int J Radiat Oncol Biol Phys*. 2004;59(1):126–37.
62. Croteau D, Scarpace L, Hearshen D, Gutierrez J, Fisher JL, Rock JP, Mikkelsen T. Correlation between magnetic resonance spectroscopy imaging and image-guided biopsies: semiquantitative and qualitative histopathological analyses of patients with untreated glioma. *Neurosurgery*. 2001;49(4):823–9.
63. Chan AA, Lau A, Pirzkall A, Chang SM, Verhey LJ, Larson D, McDermott MW, Dillon WP, Nelson SJ. Proton magnetic resonance spectroscopy imaging in the evaluation of patients undergoing gamma knife surgery for Grade IV glioma. *J Neurosurg*. 2004;101(3):467–75.
64. Burtcher IM, Skagerberg G, Geijer B, Burtcher IM, Skagerberg G, Geijer B, Englund E, Stahlberg F, Holtas S. Proton MR spectroscopy and preoperative diagnostic accuracy: an evaluation of intracranial mass lesions characterized by stereotactic biopsy findings. *AJNR Am J Neuroradiol*. 2000;21(1):84–93.
65. Hu LS, Baxter LC, Smith KA, Feuerstein BG, Karis JP, Eschbacher JM, Coons SW, Nakaji P, Yeh RF, Debbins J, Heiserman JE. Relative cerebral blood volume values to differentiate high-grade glioma recurrence from post-treatment radiation effect: direct correlation between image-guided tissue histopathology and localized dynamic susceptibility-weighted contrast-enhanced perfusion MR imaging measurements. *AJNR Am J Neuroradiol*. 2009;30(3):552–8.
66. Meijer OW, Vandertop WP, Baayen JC, Slotman BJ. Single-fraction vs. fractionated linac-based stereotactic radiosurgery for vestibular schwannoma: a single-institution study. *Int J Radiat Oncol Biol Phys*. 2003;56(5):1390–6.
67. Chopra R, Kondziolka D, Niranjan A, Lunsford LD, Flickinger JC. Long-term follow-up of acoustic schwannoma radiosurgery with marginal tumor doses of 12 to 13 Gy. *Int J Radiat Oncol Biol Phys*. 2007;68(3):845–51.
68. Hayhurst C, Zadeh G. Tumor pseudoprogression following radiosurgery for vestibular schwannoma. *Neuro Oncol*. 2012;14(1):87–92.
69. Nagano O, Serizawa T, Higuchi Y, Matsuda S, Sato M, Yamakami I, Okiyama K, Ono J, Saeki N. Tumor shrinkage of vestibular schwannomas after Gamma Knife surgery: results after more than 5 years of follow-up. *J Neurosurg*. 2010;113(Suppl):122–7.
70. Han JH, Kim DG, Chung HT, Paek SH, Park CK, Kim CY, Hwang SS, Park JH, Kim YH, Kim JW, Kim YH, Song SW, Kim IK, Jung HW. The risk factors of symptomatic communicating hydrocephalus after stereotactic radiosurgery for unilateral vestibular schwannoma: the implication of brain atrophy. *Int J Radiat Oncol Biol Phys*. 2012;84(4):937–42.
71. Dhople AA, Adams JR, Maggio WW, Naqvi SA, Regine WF, Kwok Y. Long-term outcomes of Gamma Knife radiosurgery for classic trigeminal neuralgia: implications of treatment and critical review of the literature. *J Neurosurg*. 2009;111(2):351–8.
72. Regis J, Metellus P, Hayashi M, Roussel P, Donnet A, Bille-Turc F. Prospective controlled trial of gamma knife surgery for essential trigeminal neuralgia. *J Neurosurg*. 2006;104(6):913–24.
73. Massager N, Abeloos L, Devriendt D, Op de Beeck M, Levivier M. Clinical evaluation of targeting accuracy of gamma knife radiosurgery in trigeminal neuralgia. *Int J Radiat Oncol Biol Phys*. 2007;69(5):1514–20.
74. Pollock BE, Flickinger JC, Lunsford LD, Bissonette DJ, Kondziolka D. Factors that predict the bleeding risk of cerebral arteriovenous malformations. *Stroke*. 1996;27(1):1–6.
75. Colombo F, Pozza F, Chierago G, Casentini L, De Luca G, Francescon P. Linear accelerator radiosurgery of cerebral arteriovenous malformations: an update. *Neurosurgery*. 1994;34(1):14–20.
76. Ellis TL, Friedman WA, Bova FJ, Kubilis PS, Buatti M. Analysis of treatment failure after radiosurgery for arteriovenous malformations. *J Neurosurg*. 1998;89(1):104–10.
77. Flickinger JC, Kondziolka D, Maitz AH, Lunsford LD. An analysis of the dose-response for arteriovenous malformation radiosurgery

- and other factors affecting obliteration. *Radiother Oncol.* 2002; 63(3):347–54.
78. Maruyama K, Kawahara N, Shin M, Tago M, Kishimoto J, Kurita H, Kawamoto S, Morita A, Kirino T. The risk of hemorrhage after radiosurgery for cerebral arteriovenous malformations. *N Engl J Med.* 2005;352(2):146–53.
79. Kondziolka D, Lundsford LD, Flickinger JC. Gamma knife stereotactic radiosurgery for cerebral vascular malformations. In: Aleksander E, Loeffler JS, Lundsford LD, editors. *Stereotactic radiosurgery*. New York: McGraw-Hill; 1993. p. 136–46.
80. Colombo F, Benedetti A, Pozza F, Marchetti C, Chiarego G. Linear accelerator radiosurgery of cerebral arteriovenous malformations. *Neurosurgery.* 1989;24(6):833–40.
81. Spiegelmann R, Friedman WA, Bova FJ. Limitations of angiographic target localization in planning radiosurgical treatment. *Neurosurgery.* 1992;30(4):619–23.
82. Kondziolka D, Lunsford LD, Kanal E, Talagala L. Stereotactic magnetic resonance angiography for targeting in arteriovenous malformation radiosurgery. *Neurosurgery.* 1994;35(4):585–90.
83. Gemmete JJ, Chaudhary N, Pandey AS, Oweis Y, Thompson BG, Maher CO, Gandhi D, Ansari SA. Initial experience with a combined multidetector CT and biplane digital subtraction angiography suite with a single interactive table for the diagnosis and treatment of neurovascular disease. *J Neurointerv Surg.* 2013;5(1): 73–80.
84. Stancanello J, Cavedon C, Francescon P, Causin F, Avanzo M, Colombo F, Cerveri P, Ferrigno G, Uggeri F. BOLD fMRI integration into radiosurgery treatment planning of cerebral vascular malformations. *Med Phys.* 2007;34(4):1176–84.
85. Koga T, Maruyama K, Kamada K, Ota T, Shin M, Itoh D, Kunii N, Ino K, Terahara A, Aoki S, Masutani Y, Saito N. Outcomes of diffusion tensor tractography-integrated stereotactic radiosurgery. *Int J Radiat Oncol Biol Phys.* 2012;82(2):799–802.
86. Guo WY, Wu YY, Wu HM, Chung WY, Kao YH, Yeh TC, Shiau CY, Pan DH, Chang YC, Hsieh JC. Toward normal perfusion after radiosurgery: perfusion MR imaging with independent component analysis of brain arteriovenous malformations. *AJNR Am J Neuroradiol.* 2004;25(10):1636–44.

Principles and Practice of Stereotactic Radiosurgery

Chin, L.S.; Regine, W.F. (Eds.)

2015, XVII, 842 p. 351 illus., 141 illus. in color.,

Hardcover

ISBN: 978-1-4614-8362-5